PLOS ONE

RESEARCH ARTICLE

Preservation of cellular nano-architecture by the process of chemical fixation for nanopathology

Xiang Zhou[1☯], Scott Gladstein[1☯], Luay M. Almassalha[1,2], Yue Li[1], Adam Eshein[1], Lusik Cherkezyan[1], Parvathi Viswanathan[1], Hariharan Subramanian[1], Igal Szleifer[1], Vadim Backman[1]*

1 Department of Biomedical Engineering, Northwestern University, Evanston, IL, United States of America, **2** Medical Scientist Training Program, Feinberg School of Medicine, Northwestern University, Chicago, IL, United States of America

☯ These authors contributed equally to this work.
* v-backman@northwestern.edu

Citation: Zhou X, Gladstein S, Almassalha LM, Li Y, Eshein A, Cherkezyan L, et al. (2019) Preservation of cellular nano-architecture by the process of chemical fixation for nanopathology. PLoS ONE 14 (7): e0219006. https://doi.org/10.1371/journal.pone.0219006

Editor: Etienne Dague, LAAS-CNRS, FRANCE

Received: February 5, 2019

Accepted: June 13, 2019

Published: July 22, 2019

Data Availability Statement: All relevant data are within the manuscript and Supporting Information files.

Funding: This work was supported by National Institutes of Health (NIH) grants R01CA155284, R01CA200064 and R01CA165309, National Science Foundation (NSF) grant EFMA-1830961, and Lungevity Foundation. The funders had no role in study design, data collection and analysis, decision to publish, or preparation of the manuscript.

Abstract

Transformation in chromatin organization is one of the most universal markers of carcinogenesis. Microscale chromatin alterations have been a staple of histopathological diagnosis of neoplasia, and nanoscale alterations have emerged as a promising marker for cancer prognostication and the detection of predysplastic changes. While numerous methods have been developed to detect these alterations, most methods for sample preparation remain largely validated via conventional microscopy and have not been examined with nanoscale sensitive imaging techniques. For these nanoscale sensitive techniques to become standard of care screening tools, new histological protocols must be developed that preserve nanoscale information. Partial Wave Spectroscopic (PWS) microscopy has recently emerged as a novel imaging technique sensitive to length scales ranging between 20 and 200 nanometers. As a label-free, high-throughput, and non-invasive imaging technique, PWS microscopy is an ideal tool to quantify structural information during sample preparation. Therefore, in this work we applied PWS microscopy to systematically evaluate the effects of cytological preparation on the nanoscales changes of chromatin using two live cell models: a drug-based model of Hela cells differentially treated with daunorubicin and a cell line comparison model of two cells lines with inherently distinct chromatin organizations. Notably, we show that existing cytological preparation can be modified in order to maintain clinically relevant nanoscopic differences, paving the way for the emerging field of nanopathology.

Introduction

Over the past few decades, despite a tremendous amount of research into discovering new molecular targets and improving precision therapies, cancer remains a leading cause of death worldwide. For almost all types of cancer, treatment effectiveness is directly associated with

Competing interests: I have read the journal's policy and the authors of this manuscript have the following competing interests: Drs. Backman and Subramanian are cofounders/shareholders of Nanocytomics LLC. This does not alter our adherence to PLOS ONE policies on sharing data and materials.

the stage of detection [1]. Although for low-prevalence malignancies therapeutics remains the primary option for the management of the disease, for more prevalent malignancies such as lung, colon, prostate, and ovarian cancers both the health care costs and mortality rates can be greatly reduced via the development of two-tiered screening strategy. Two-tier screening starts with a cost-effective, patient-compliant, ideally non-invasive or only minimally invasive test that can be administered in the primary care setting and has a sufficiently high sensitivity for clinically significant and treatable lesions. Patients risk-stratified based on this first-tier test may then undergo a follow up examination using the more definitive second-tier test. A notable example of the two-tier screening is the pap-smear as a pre-screen for colposcopy paradigm for cervical cancer screening, which after its introduction in clinical care in the 1950s has reduced cervical cancer mortality by more than 95% in the screening population. However, the development of two-tier screening for non-cervical malignancies has been challenging. To date, most attempts to develop this two tier screening methodology have focused on identifying specific molecular transformations correlated with tumor development, with genomic and proteomic markers acting as the two major sources investigated as potential biomarkers [2]. While molecular screening is promising, the heterogeneous accumulation of genetic, epigenetic, and proteomic transformations associated with tumorigenesis make the use of individual markers for screening limited across a wide population. On the other hand, at the later stages of tumorigenesis (e.g. dysplasia and malignancy) these divergent molecular alterations are near universally convergent on microscopic structural alterations that can be identified by the well-established cytological examination. Owing to this convergence between molecular and structural alterations, a number of technologies have been utilized for the detection of early stage nanoscopic structural alterations: single molecule localization microscopy [3], quantitative phase imaging [4], spatial light interference microscopy [5], partial wave spectroscopic (PWS) microscopy [6], low-coherence enhanced backscattering spectroscopy [7], enhanced backscattering spectroscopy [8], transmission electron microscopy [9], and angle-resolved low-coherence interferometry [10]. In these approaches, alterations in nanoscopic ultrastructure act as a convergence point between these numerous independent molecular transformations that are detected by the two-tier screening approach.

As with any cytological microscopy techniques, cells must first undergo fixation and processing in order to maintain their structural stability for long term storage and imaging. Since these preparatory steps are known to have detrimental effects to the cellular structure at the micron-scale, improper preparation could result in nanoscopic distortion and loss of sensitivity to underlying ultrastructural transformations that occur during early carcinogenesis. PWS microscopy was developed as a label-free, non-invasive optical method to measure nanoscopic changes in cells by analyzing the variations in back-scattered light [6]. In previous work, live-cell PWS microscopy has demonstrated success in visualizing and quantifying cellular changes during chemical fixation, showing that nanoscale structural information can be preserved during chemical fixation methods [11]. Here, we further extended its application to track cellular structure changes during all stages of nanocytological preparation. In particular, we test the effects of a number of common cytological preparations on the ultrastructure of cell lines using base-line live cell measurements as controls. This access into nanoscopic information during all preparation steps starting at live cells allows a generalized frame-work to assess the maintenance of ultra-structure during the preparation of biological samples at all stages of cytological prep: fixation, rehydration and staining. Critically, we find that while some information is lost during nanocytological preparation, clinically relevant information can be relatively well preserved and applied for nanocytological applications. Thus, the process presented here can be utilized for systematic validation of methods to enable detection of nanoscale

structural alterations in human disease to verify that the measured structures represent those underlying pathological process found in live cells.

Material and methods

Live cell models

Two models were developed for the analysis of cytological preparation on cellular ultrastructure. The first is a drug-based model of Hela cells differentially treated with 10μM daunorubicin for 15 minutes in order to induce alterations in higher-order chromatin structure potentially due to nucleosomal eviction [12]. The second is a cell line comparison model of two cell lines with inherently distinct chromatin organizations. The two cell lines compared are originally derived from A2780 and A2780.m248 lines (STR profiles included in SI). For each model, nanoscopic changes in chromatin folding were detected and quantified by live-cell PWS microscopy prior to nanocytological preparation.

Cell culture

HeLa cells, A2780 and A2780.m248 (M248) were grown in freshly prepared RPMI-1640 media (Life Technologies) supplemented with 10% (vol/vol) FBS (Sigma-Aldrich) and grown at 37˚C and 5% CO_2. HeLa cells were sourced from ATCC, CCL-2. A2780 and A2780.M248 cell lines were a gift from C.-P. Huang Yang and were obtained from the lab of E. de Vries at Albert Einstein College of Medicine. All of the cells in this study were maintained between passage 5 and 30. Microscopy measurements were obtained from cells grown on uncoated size 1 glass coverslips attached to 50mm petri dishes (Cell Vis). Petri dishes were seeded with between 10,000 and 50,000 cells in 2ml of the cell appropriate media at the time of passage. Cells were allowed at least 24 hours to re-adhere and recover from trypsin-induced detachment. Imaging was performed when the surface confluence of the slide was between 50–70% and when cells were in the cell culture media. A reference scattering spectra was obtained from an open surface of the substrate coverslip immersed in media to normalize the intensity of light scattered for each wavelength at each pixel.

Chemical fixation

After live cell imaging, cell culture media was removed from the petri-dish and cells were washed with 2mL phosphate buffered saline solution twice. After removal of the washing solution, 2mL of specified fixative solution was added into the dish. Six common fixatives were tested in our study: 1. acetic acid: ethanol = 1:3 (v/v%); 2. Carnoy's fixative (Ethanol : chloroform : acetic acid = 6:3:1 (v/v%)); 3. FAA fixative (Ethanol : formaldehyde : acetic acid = 16:3:1 (v/v%)); 4. 4% formaldehyde in PBS solution (pH~7.4); 5. 2.5% glutaraldehyde and 2% formaldehyde in PBS solution (pH~7.4). 6. 95% ethanol (v/v%). After 15 minutes of fixation at room temperature, the cells were imaged in the fixative solution. A reference spectra of the coverslip immersed in the specified fixatives solution was obtained for normalization.

Serial rehydration

After the 95% ethanol fixation, cells were sequentially rehydrated with 2mL of 70%, 50%, 25% ethanol solution and DI water for 10 minutes each under room temperature. The same cells were imaged in the specified solution after each step of rehydration. For comparison, cells were directly rehydrated with DI water after 95% ethanol fixation and were imaged in DI water after 30 minutes. After each step of imaging, a reference spectrum of the coverslip immersed in the specified solution was obtained for normalization.

Air drying

After serial rehydration, DI water was removed from the petri-dish and 100mM trehalose-water solution was added into the petri-dish as a drying solution. Trehalose is hypothesized to prevent cell shrinkage and protect cell membranes by forming high-viscosity glass matrix during evaporation of solvents. It has been reported that cells with intracellular trehalose has improved tolerance against freezing and desiccation [13, 14]. In our study, since cells were fixed and their membrane integrity was no longer maintained, trehalose will penetrate into cells by diffusion and serve as structural protection molecules during air drying. After a 30-minute treatment, trehalose solution was completely removed from the petri-dish by pipetting. Cells were then air dried at room temperature for 48 hours. In addition, we investigated the effects of air drying speed on chromatin organization as measured by PWS. For humidity-controlled air drying, cells were air dried without trehalose treatment under three humidity conditions (25%, 50% and 75%) at room temperature. After air drying, cells were imaged in 95% ethanol. A reference spectra of the coverslip immersed in the 95% ethanol solution was obtained for normalization.

Traditional histological staining

After air drying and imaging, cells were stained with Hematoxylin and Cyto-Stain (Thermo Scientific, Richard-Allan Scientific) in the petri-dish. The staining process consisted of washing with DI water for 60 seconds, staining with Hematoxylin II for 25 seconds, washing with DI water for 15 seconds, washing with clarifier for 45 seconds, washing with DI water for 30 seconds, washing with bluing reagent for 25 seconds, washing with DI water for 30 seconds, washing with 95% ethanol for 30 seconds, staining with Cyto-Stain for 25 seconds and final washing with 95% ethanol for 60 seconds. After staining, the same cell populations were imaged again in 95% ethanol. A reference spectra of the coverslip immersed in the 95% ethanol solution was obtained for normalization.

Immunofluorescence staining

The immunofluorescence staining was performed on HeLa model. The staining process consisted of: 10 minute PFA fixation (4% formaldehyde in PBS solution, Electron Microscopy Sciences), washing with PBS solution, blocking and permeabilization (1% BSA and 0.1% Triton X-100 in PBS) for 20 minutes, washing with PBS solution, incubation with primary antibody (Anti-Histone H3K9 me3, Abcam) in blocking solution at 4˚C overnight, washing with blocking solution, incubation with secondary antibody (Goat anti mouse Alexa Fluor 488) in blocking solution for 2 hours and final washing with PBS solution. Hoechst 33342 staining was performed after the immunofluorescent preparation for co-localization. PWS measurements of the same cells were taken in PBS solution after each wash step and a reference spectra of the coverslip immersed in the PBS solution was obtained for normalization. Fluorescent images of the same cells was performed at the end of the preparation.

Immunofluorescence staining for STORM/PALM nanoscopic imaging

The immunofluorescence staining was performed on the A2780/M248 cell line model. The staining process consisted of 10 minute PFA fixation (4% formaldehyde in PBS solution, Electron Microscopy Sciences), washing with PBS solution, reduction in 0.5% sodium borohydride in PBS to reduce auto-fluorescence from the background, blocking and permeabilization (1% BSA and 0.1% Triton X-100 in PBS) for 20 minutes, washing with PBS solution, incubation with primary antibody (Anti-RNA polymerase II, Abcam) in blocking solution at 4˚C

overnight, washing with blocking solution, incubation with secondary antibody (Alexa Fluor 546) in blocking solution for 2 hours and final washing with PBS solution. PWS measurements of the same cells were taken in PBS solution after each wash step and a reference spectra of the coverslip immersed in the PBS solution was obtained for normalization. STORM imaging was performed at the end of the preparation.

Results

PWS imaging of live cell models

At any given intracellular location, refractive index n is proportional to the local macromolecular density (proteins, DNA, RNA, etc.) (ρ): $n = n_{water}+\alpha\rho$ with α the refraction increment, which is nearly constant for most kinds of macromolecules [15]. Spatial variations in refractive index result in light scattering, and thus variations in cellular (e.g. chromatin) density can be assessed through the analysis of light scattering properties of a cell. Live-cell PWS microscopy measures the optical interference signal of the backscattering light that is produced by spatial variations of refractive index [16–18]. By quantifying the standard deviation (Σ) of the spectra acquired by PWS microscopy, PWS obtains subdiffractional information from cellular structures, in particular the internal structures of nucleus. Σ is a measure of the heterogeneity of macromolecular density and is proportional to key metrics of nanoscale organization: the standard deviation of the spatial variations of molecular density ($\delta\rho$) and either the molecular correlation length or the scaling exponent of the mass of chromatin (D): $\Sigma\propto(D-D_0)\delta\rho$, where D_0~1.5 [17, 18]. $\delta\rho$ is related to the volume fraction of molecular crowders φ: $\delta\rho \propto \sqrt{(1-\varphi)\varphi}$. D characterizes the type of scaling between the mass of chromatin (M) contained within a sphere of radius R: $M\propto R^D$; $D<3$ for fractal scaling (in which case D is referred to as the mass fractal dimension), which is typical for polymeric structures such as chromatin. Length scale sensitivity of PWS depends on the illumination and light collection geometry of the microscope and is typically optimized to sense the chromatin length scales that correspond to the supranucleosomal chromatin structure from the size of chromatin chains to the size of topologically associated domains are the most significantly altered in early carcinogenesis (20-350nm; from ~1kb to 1–10Mbp) [9, 17, 19]. PWS generates an image of a cell such that for each diffraction-limited pixel within the cell nucleus nanoscale heterogeneity of chromatin packing is measured as either Σ or D.

For clinical diagnostic applications, the use of live cells is problematic and fixed cytology or histology specimens are more often used. To study nano-cytological preparation protocols to preserve the nanoscopic chromatin structure, two cell line models were imaged by live-cell PWS at live state as controls (Fig 1A and 1B). The cell nuclei in each group were segmented for mean nuclear Σ quantification. The mean nuclear Σ was normalized and rescaled to 100% on average with respect to the appropriate control group to isolate the effects of our cell preparation protocols (untreated HeLa cells and A2780 cells for all cytological conditions). The mean nuclear Σ of HeLa cells showed a 31% decrease after the 15min 10μM daunorubicin treatment as compared to the control group ($P < 0.001$, HeLa-control = 201 cells, HeLa-daunorubicin = 200 cells). Conversely, the mean nuclear Σ of M248 displayed a 17% increase as compared to the wild-type A2780 ($P < 0.001$, M248 = 240 cells, A2780 = 228 cells) (Fig 1C). As these alterations in higher-order chromatin organizations ($\Delta\Sigma$) are introduced by distinct mechanisms, they can act as molecularly distinct models of nanoscopic changes of chromatin topology to assess the effects of nanocytological preparation.

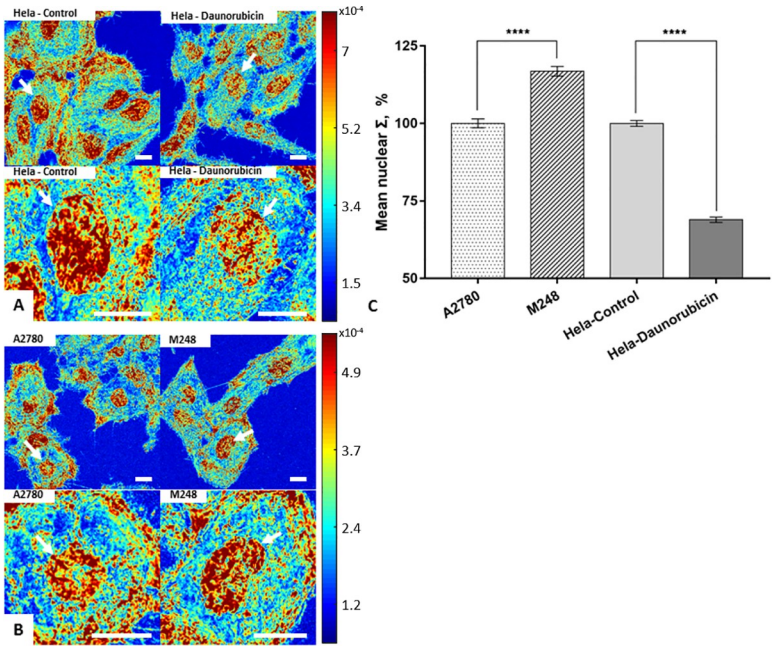

Fig 1. Molecularly distinct structural models of nanoscopic changes to chromatin topology. (A) Representative Σ maps of HeLa cells before and 15 min after daunorubicin treatment. (B) M248 and A2780. (C) Quantification of mean nuclear Σ change in HeLa model before and 15 min after daunorubicin treatment (HeLa-control = 201 cells, HeLa-daunorubicin = 200 cells), and in the A2780/M248 cell line model (M248 = 240 cells, A2780 = 228 cells) with SE bars. All scale bars are 14μm. **** $p<0.001$.

https://doi.org/10.1371/journal.pone.0219006.g001

Effects of different chemical fixation methods on nuclear structure

To determine the effects of chemical fixation methods on our structural models, the same cell populations were imaged before and after fixation, and their mean nuclear Σ was quantified. For 95% ethanol fixation, slight morphological changes were observed after 15 minutes, but the cell nucleus remained clear and detectable in both models. The ΔΣ was quantified to be ~20% for HeLa model ($P < 0.001$, HeLa-control = 141 cells, HeLa-daunorubicin = 145 cells), and ~17% ($P < 0.001$, M248 = 110 cells, A2780 = 115 cells) for the A2780/M248 cell line model (Fig 2). Our results showed that the nanoscopic structural differences (ΔΣ) between populations in both models remained significant during 95% ethanol fixation. Although the population difference was preserved after fixation, on the single cell level, we found a weak correlation between nuclear structure before and after fixation (Pearson correlation coefficient (PPC) = ~ 0.4) (S1 Fig). This implies that during fixation different individual nucleus could undergo very different structural transformations, such that the single cell level difference might not be reliably detectable after fixation. In addition, we tested five fixatives that were commonly used in traditional histology studies or immunofluorescent microscopy. As can be seen from Fig 3, the crosslinking fixatives, formaldehyde (HeLa-control = 91 cells, HeLa-daunorubicin = 89 cells) and glutaraldehyde (HeLa-control = 92 cells, HeLa-daunorubicin = 96 cells) were able to preserve the ΔΣ, while other fixatives that contain acetic acid resulted in ΔΣ loss after 15 minutes of fixation (Acetic acid + Ethanol, HeLa-control = 78 cells, HeLa-daunorubicin = 77 cells; Carnoy's fixative, HeLa-control = 29 cells, HeLa-daunorubicin = 35 cells; FAA fixative, HeLa-control = 40 cells, HeLa-daunorubicin = 39 cells). Since 95% ethanol is a standard cytological fixative and is stable over longer periods than the other fixatives, the subsequent nanocytology protocols (rehydration, air drying and traditional histological staining)

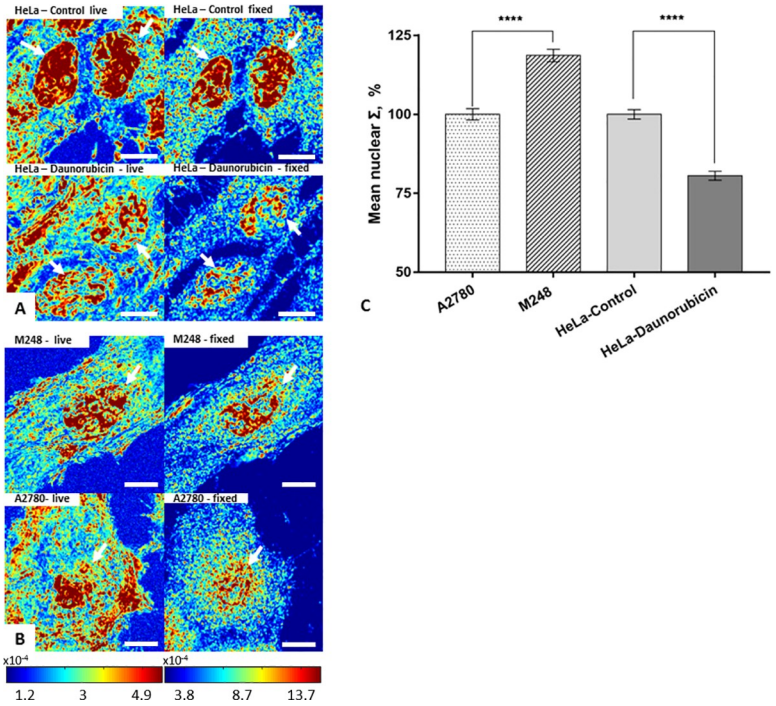

Fig 2. Preservation of ΔΣ by 95% ethanol fixation in two structural cell line models. (A) Control and daunorubicin treated HeLa cells before and after 95% ethanol fixation. (B) M248 and A2780 cells before and after 95% ethanol fixation. (C) Quantification of mean nuclear Σ difference in HeLa cell model (HeLa-control = 141 cells, HeLa-daunorubicin = 145 cells), and in the A2780/M248 cell line model after 95% ethanol fixation (M248 = 110 cells, A2780 = 115 cells) with SE bars. All scale bars are 10μm. **** $p<0.001$.

https://doi.org/10.1371/journal.pone.0219006.g002

were developed and tested based on 95% ethanol fixation. On the other hand, crosslinking fixation was used for immunofluorescent labeling as the most common approach.

Serial rehydration

Although 95% ethanol preserves the ΔΣ, it could cause cell shrinkage and aggregation especially when cells were freely suspended in solution. To address this problem, we rehydrated the 95% ethanol-fixed cells with gradually decreasing concentrations of ethanol. PWS images of the same cells were acquired at each ethanol concentration condition during the rehydration process. For both structural models, we observed a slight increase in Σ in cytoplasmic regions after serial rehydration, but the cell nucleus remained detectable throughout the whole process (Fig 4B and 4C, S2B and S2C Fig). By quantifying the mean nuclear Σ in each step of rehydration (Fig 4A and S2A Fig), we found that the structural differences (ΔΣ) in both models were well preserved (HeLa-control = 125 cells, HeLa-daunorubicin = 125 cells, M248 = 61 cells, and A2780 = 67 cells). In comparison to this serial rehydration, a direct rehydration from 95% ethanol fixation to DI water was also tested on HeLa model (Fig 4D and 4E) and resulted in a total loss of measureable differences between the samples (HeLa-control = 42 cells and HeLa-daunorubicin = 46 cells). This differential response in structure to the solvation suggests that a rapid shifts in the osmotic pressure by switching solvents could alter the observed differences in the chromatin structure.

Preservation of ultrastructure during air drying

Air drying is a common preparatory process in cytology because it allows the adhesion of cells to the substrate and stabilizes cellular structures onto the glass substrate. However, air drying

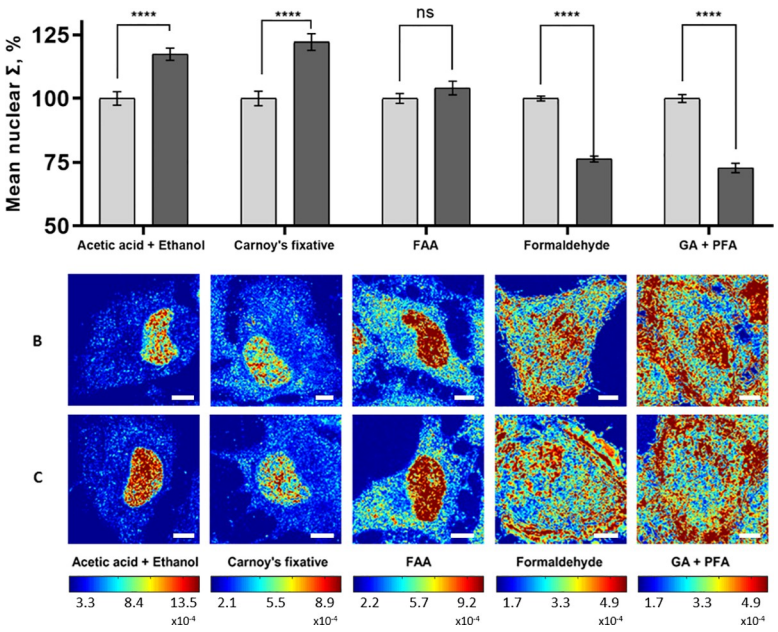

Fig 3. Commonly used fixatives and their effects on ΔΣ in HeLa model. (A) Quantification of mean nuclear Σ in HeLa-control (grey columns) and HeLa-daunorubicin (black columns) before and after fixation using five different fixatives: 1. acetic acid: ethanol = 1:3 (v/v%), HeLa-control = 78 cells, HeLa-daunorubicin = 77 cells; 2. Carnoy's fixative (Ethanol : chloroform : acetic acid = 6:3:1 (v/v%)), HeLa-control = 29 cells, HeLa-daunorubicin = 35 cells; 3. FAA fixative (Ethanol : formaldehyde : acetic acid = 16:3:1 (v/v%)), HeLa-control = 40 cells, HeLa-daunorubicin = 39 cells; 4. 4% formaldehyde in PBS solution (pH~7.4), HeLa-control = 91 cells, HeLa-daunorubicin = 89 cells; 5. 2.5% glutaraldehyde and 2% formaldehyde in PBS solution (pH~7.4), HeLa-control = 92 cells, HeLa-daunorubicin = 96 cells. (B) Representative PWS images of HeLa-control (top row), HeLa-daunorubicin (bottom row) fixed by different fixatives. All scale bars are 8μm. **** $p<0.001$.

https://doi.org/10.1371/journal.pone.0219006.g003

is also known to cause cell volume changes as well as internal structural distortions. To preserve the nanoscopic structural information for PWS imaging after the process of air drying, we treated the rehydrated cells with trehalose solution for 30 minutes before air drying. After 48-hour air drying, the same cell populations were imaged again in 95% ethanol solution (Fig 4A and 4B), and their mean nuclear Σ was quantified (Fig 5). Our results suggest that air drying from trehalose solution maintained the cell morphology and preserved the ΔΣ in both models (~20% for Hela model, $P<0.001$, HeLa-control = 151 cells, HeLa-daunorubicin = 140 cells and ~12% for the A2780/M248 cell line model, $P<0.001$, M248 = 62 cells, A2780 = 60 cells). The preservation of ΔΣ could be explained by the formation of highly viscous trehalose glass inside the cells which immobilized the macromolecules and stabilized the internal structures during evaporation of water. In comparison, we investigated the effects of direct air drying under different humidity conditions without trehalose treatment. As can be seen in S3 Fig, air drying in low (~25%) and medium (~50%) humidity condition preserved the ΔΣ, but they both resulted in substantial morphological changes and great reduction in ΔΣ (25% humidity, HeLa-control = 67 cells, HeLa-daunorubicin = 72 cells; 50% humidity, HeLa-control = 131 cells, HeLa-daunorubicin = 141 cells; 75% humidity, HeLa-control = 135 cells, HeLa-daunorubicin = 126 cells). This result indicates that direct air drying which would be detrimental to preservation of cellular ultrastructures.

Histological staining

After air drying from trehalose solution, we stained the two cell line models with Hematoxylin and Cyto-Stain. In histology, Hematoxylin is a commonly used nuclei stain and Cyto-Stain is

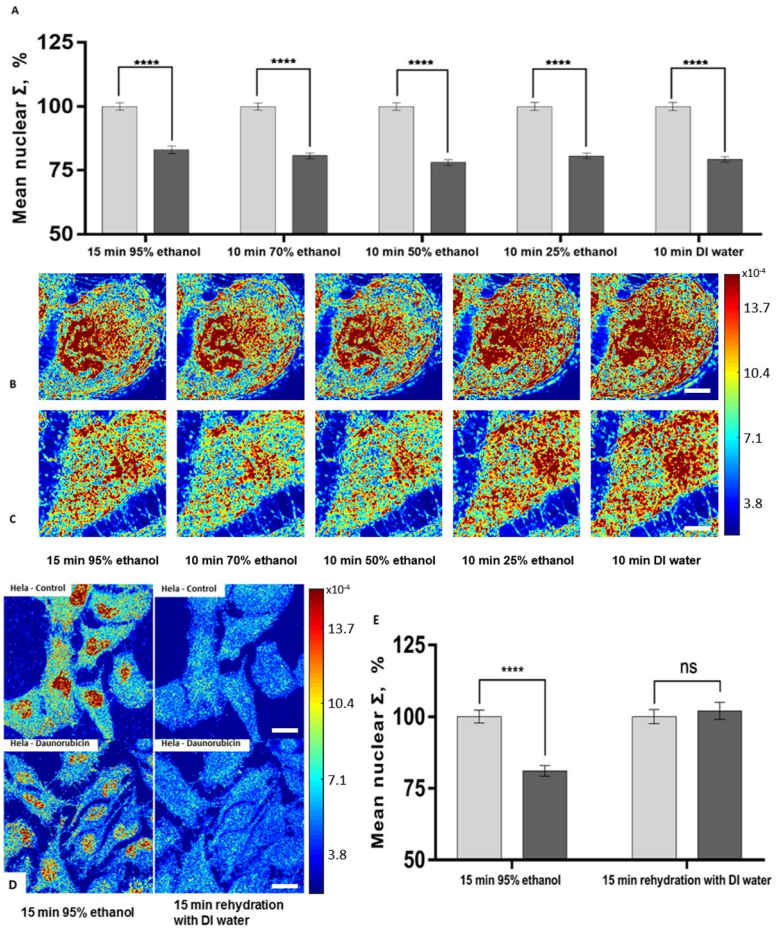

Fig 4. The effects of rehydration on ΔΣ in the HeLa cell model. Quantification of Σ in (A) HeLa-control (grey columns; 125 cells) and HeLa-daunorubicin (black columns; 125 cells) after each step of serial rehydration with SE bars. The ΔΣ was preserved during serial rehydration. Representative PWS images of the same HeLa cells [control (B) and daunorubicin treated (C)] after each step of serial rehydration. Scale bars are 10μm. (D) Direct rehydration was performed on HeLa model, and the same cells were imaged by PWS before and after direct hydration with DI water. Scale bars are 22μm.(E) Quantification of Σ in HeLa-control (grey columns; 42 cells) and HeLa-daunorubicin (black columns; 46 cells) showing the loss of ΔΣ after direct rehydration. **** $p<0.001$.

https://doi.org/10.1371/journal.pone.0219006.g004

mix of dyes used for polychromatic staining. The staining process consists of multiple steps (see M&M) which might alter the chromatin organizations. To verify that the staining process does not result in a loss in diagnostic performance, we imaged the same cell populations with PWS microcopy throughout all stages. As can be seen in Fig 6, the process of staining results in a clearer demarcation of the nucleus while maintaining diagnostic differences (ΔΣ) were preserved for both models (HeLa-control = 82 cells, HeLa-daunorubicin = 75 cells, $p<0.001$); M248 = 73 cells, A2780 = 76 cells, $p<0.001$). However, the reduction in the size of ΔΣ in both models also indicate that the staining process could cause structural information loss.

Immunofluorescent labeling

Immunofluorescence (IF) staining is a widely used technique that allows target structures to be visualized and located by light microscopy. In recent years, although many improvements in fluorophores and detection methods have been made, the major procedures of immunofluorescent labeling remained unchanged. These procedures, including chemical fixation,

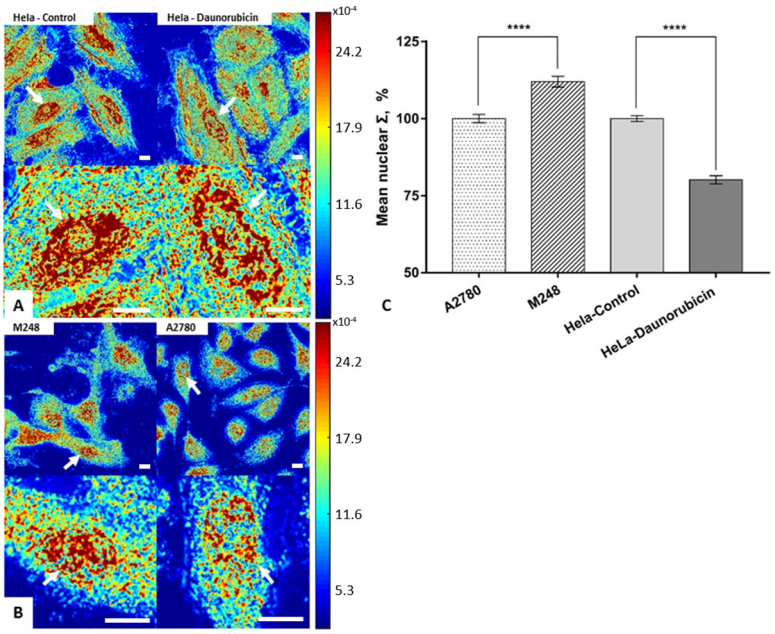

Fig 5. Preservation of ΔΣ after air drying from trehalose solution in two structural cell line models. (A) HeLa model and (B) the A2780/M248 cell line model imaged by PWS after air drying. (C) Quantification of mean nuclear Σ in HeLa cell model (HeLa-control; 151 cells, HeLa-daunorubicin; 140 cells), and in the A2780/M248 cell line model (M248; 62 cells, A2780; 60 cells) with SE bars. All scale bars are 9μm. **** $p<0.001$.

https://doi.org/10.1371/journal.pone.0219006.g005

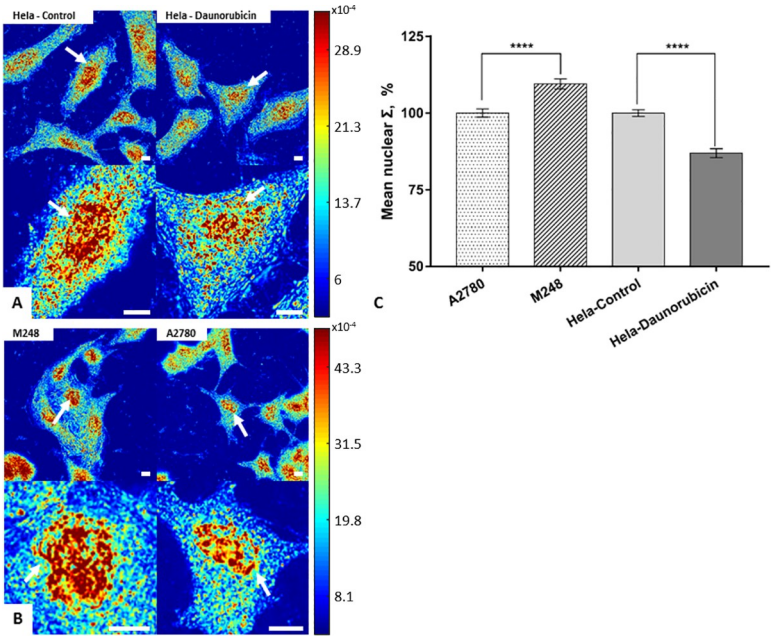

Fig 6. Effects of Hematoxylin and Cyto-Stain on ΔΣ in two structural cell line models. Representative PWS images of HeLa model (A) and the A2780/M248 cell line model (B) after staining. (C) Quantification of mean nuclear Σ in HeLa model (HeLa-control; 82 cells, HeLa-daunorubicin; 75 cells), and in the A2780/M248 cell line model (M248; 73 cells, A2780; 76 cells) with SE bars. All scale bars are 7μm. **** $p<0.001$.

https://doi.org/10.1371/journal.pone.0219006.g006

blocking, permeabilization, antibody incubation and multiple steps of washing, are known to cause structural distortions in the cell. Here, we performed PWS imaging at each step of the fluorescent labeling to study the nanoscale changes in chromatin organization. Fluorescent and STORM images were also acquired at the end of the preparation to verify the labeling process (Figs 7 and 8). Quantitatively, the structural differences ($\Delta\Sigma$) in both models were preserved during each preparatory step (HeLa-control = 72 cells, HeLa-daunorubicin = 78 cells, M248 = 63 cells, and A2780 = 71 cells). Cell morphology was maintained. Further, we performed co-localization analysis of PWS and fluorescent images on HeLa model (Fig 7D). Since the cells were labeled with anti-H3K9me3 antibody which is an indicator of the heterochromatin and denser regions of the nucleus, in theory the mass density distribution of these subdivisions (as indicated by Σ) could be related to their fluorescent labeling density. To test our hypothesis, we divided the pixels within each nuclei equally into 10 subdivisions based on their fluorescent intensity rankings. And then, we calculated the relative Σ of the subdivision by the following procedure. First, the unnormalized Σ of each subdivision from a single nuclei was averaged and then normalized to the average Σ of that whole nuclei. Next, that normalized Σ for each subdivision was averaged across 316 nuclei to calculate each relative Σ. For 316 cells analyzed, the relation between fluorescent intensity and the relative nuclear Σ follows an exponential decay model ($R^2 = 0.955$):

$$\Sigma_r \propto -e^{-I_r}$$

Σ_r : Relative nuclearΣ.

I_r : Relative fluorescent intensity.

As can be seen in Fig 7E, the relative nuclear Σ (Σ_r) increases very rapidly with relative fluorescent intensity (I_r) in low I_r regions, and plateaus at around 50% I_r.

Discussion

We have developed two cell line models with nuclear structural differences to study the effects of chemical fixation and staining for nanopathological preparation for quantitative evaluation of the underlying chromatin ultrastructure. The nuclear structural differences were introduced by two different methods: chemotherapy drug treatment in the Hela model and inherent differences in the A2780/M248 cell line model. These structural differences were quantified in live cells as $\Delta\Sigma$, which can directly probe supra-nucleosomal chromatin structure and directly correlates with global patterns in gene expression [16, 20]. The two models have demonstrated stability and reproducibility, and thus enabling the systematic study of nanoscale diagnostic information changes during fixation processes both for label-free optical methods even when paired with cytological staining (Fig 6) or immunofluorescence (Fig 7). Likewise, these methods are suitable for super-resolution based microscopy for multiple chromatin markers (Fig 8). Notably, we show by direct analysis of the same cells before and after fixation, ethanol and aldehyde fixation are both able to preserve $\Delta\Sigma$ while resulting in minimal changes to the overall cellular morphology. Although it has been shown that chemical fixatives would result in both cellular composition and structural changes [21, 22], our results indicate that the relative structural information at the nanoscale could be preserved during fixation. Therefore, the detection of nanoscale changes would still be possible despite the structural transformation. In studies of the subsequent preparation procedures after ethanol fixation, we found that a gradual rehydration and controlled air drying were both necessary to maintain differences in

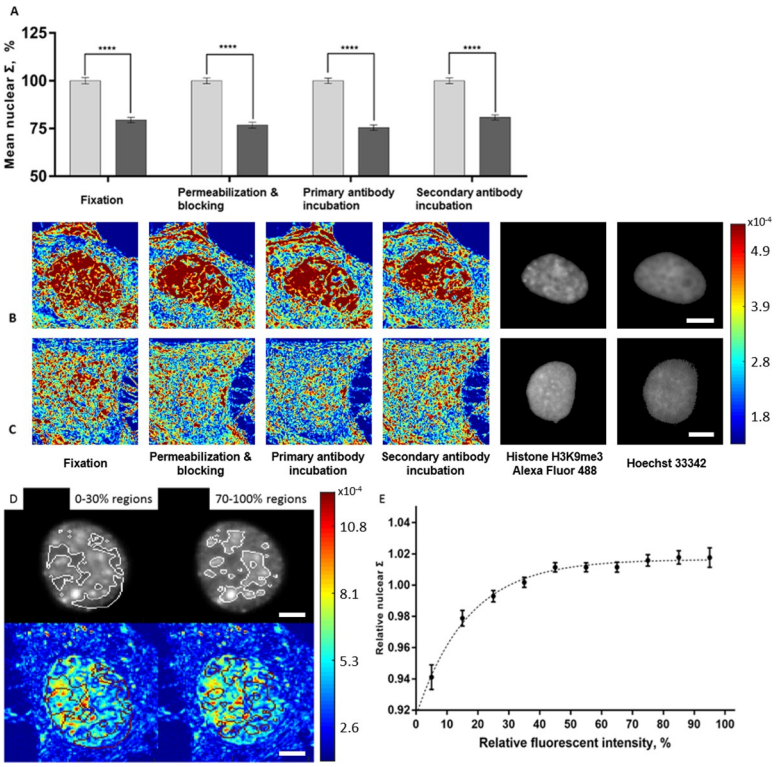

Fig 7. Effects of immunofluorescence staining on ΔΣ. HeLa cells were stained using antibody for H3K9me3 (Alexa Fluor 488). (A) Quantification of Σ in HeLa cell model (HeLa-control; 72 cells, HeLa-daunorubicin; 78 cells) at each step of immunofluorescent staining. Representative PWS (left) and fluorescent images (right) of HeLa-control (B) and HeLa-daunorubicin (C) at each step of immunofluorescent staining. (D) Colocalization using PWS and fluorescent microscopy. Each nucleus was segmented into 10 subdivisions based on their fluorescent intensity rankings. Regions with 0–30% and 70–100% fluorescent intensity rankings were shown on both fluorescent and PWS images. (E) Relationship between relative average Σ and fluorescent intensity, with standard error. For each nucleus, we calculated the relative Σ of each fluorescent subdivision by normalizing its Σ to the average Σ of the whole nucleus. The graph shows the averaged relative Σ for each fluorescent subdivision across 316 nucleus. All scale bars are 5μm. **** $p<0.001$.

https://doi.org/10.1371/journal.pone.0219006.g007

chromatin organization. Additionally, the application of histological staining and immunofluorescence can be used to demarcate the nucleus even though differences in ultra-structure are reduced between samples. This information loss could be attribute to the hydration and dehydration steps during staining which could alter the cellular structure at the nanoscale.

Besides ethanol-based fixation process, we also studied the immunofluorescent labeling process after aldehyde fixation. Immunofluorescence is a powerful tool in detecting the existence and spatial distribution of antigens. It is widely used in histopathology and is the basis for many super-resolution imaging techniques. However, the immunofluorescent labeling process involves multiple steps, which until now have not been validated rigorously between live and fixed cells at the nanoscale. It is known that these steps could largely determine the staining outcomes, but their effect on nanoscale diagnostic information was unstudied. In order to validate this process, we quantified changes in chromatin scaling of the same cells during all stages of the labeling process, and performed fluorescent microcopy and STORM at the end of the preparation. Our results show that the structural differences can be preserved during the labeling process for super-resolution imaging (Fig 8). Finally, as the underlying structure of chromatin will likely vary based on molecular alterations, we demonstrate the capacity for direct co-localization analysis of chromatin domains. Notably, we found a clear trend

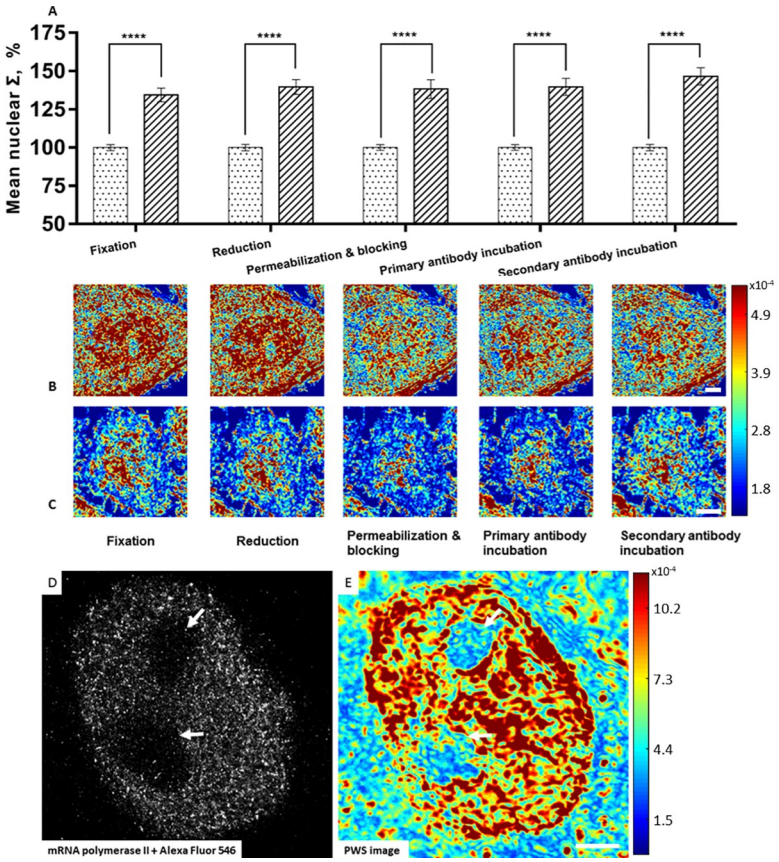

Fig 8. Effects of STORM preparation on chromatin ultrastructure. A2780 and M248 cells were stained using antibody for mRNA polymerase II (Alexa Fluor 546). (A) Quantification of Σ (M248; 63 cells, A2780; 71 cells) at each step of super resolution immunofluorescent labeling. Representative PWS images of M248 (B) and A2780 (C) at each step of fluorescent labeling. Scale bars are 6 μm. Representative STORM (D) and PWS image (E) for the same A2780 cell nuclei for verification of the nanoscopic labeling process. Scale bar is 2.5μm. Similar nuclear features can be seen on both PWS and STORM images. Arrows indicate nucleolus. **** $p<0.001$.

https://doi.org/10.1371/journal.pone.0219006.g008

between Σ and labeling density of H3K9me3 in the colocalization using PWS and fluorescent microscopy, which is frequently altered in carcinogenesis [23]. Consequently, these findings indicate that high throughput molecular-structural analysis could be useful for future nano-pathological applications. One limitation of the models used in this study is that they are both based on adherent cell lines. At this stage, the imaging of tissue samples is not applicable for the design of this study because the induced or inherent structural differences need to be validated in live cells before protocol testing. Future work will be needed to validate these protocols in other cell types, such as tissue sections, needle biopsies, and non-adherent cell lines. In sum, this work enables the future detection of nanoscale structural alterations in human disease using nanocytological preparatory methods that are verified to represent those underlying a pathological process found in live cells.

Conclusion

The emergence of imaging and molecular techniques capable of measuring the nanoscale structure of cells has the potential to greatly expand our understanding of biological function and human diseases. In the evaluation of human tissue, there are numerous preparatory steps required during the collection and processing of cells for nanoscopic analysis. Indeed, while

nanopathology will likely emerge as a major advance in the near future, these capabilities depend on validated methods that can reliably maintain nanoscopic information between live and prepared cells. In this work, we demonstrate that although fixation, immunofluorescence, and histo-pathology staining alter structural information at the nanoscale, these methods can still reliably provide nanoscopic information for multiple imaging techniques. In particular, we use a recently developed imaging technique, live-cell PWS microscopy, to systematically study the effects of fixation and other preparatory processes on nuclear structure at the nanoscale. By using two distinct cell line models, we show that the relative structural information ($\Delta\Sigma$) was well preserved during ethanol and aldehyde fixation, and during the subsequent preparatory steps required for super resolution fluorescent nanoscopy, immunofluorescent microscopy, and conventional histological examination. These findings would also be crucial for other fixed-cell based technologies with nanoscale sensitivity. In total, we developed a robust nano-cytological preparation process that can preserve the chromatin ultrastructure during all preparatory stages, from fixation to air drying, that can be applied as a standard validation for nanoscopic studies. This approach has proven effective in long term preservation of chromatin organization differences and it can be potentially applied in clinical nanoscopic studies. As this field will likely emerge due to the rapid pace of nanoscopic imaging techniques, this work provides a method to verify that studies of pathological processes extend to the structural behavior of living cells.

Supporting information

S1 Fig. Correlation between relative nuclear Σ during 95% ethanol fixation. The same cells were tracked and imaged before and after 95% ethanol fixation (HeLa-control = 71 cells, HeLa-daunorubicin = 61 cells). The relative nuclear Σ was weakly correlated, but the population difference was preserved.
(TIF)

S2 Fig. The effects of rehydration on ΔΣ in the A2780/M248 cell line model. Quantification of Σ in (A) M248 (columns with dots; 61 cells) and A2780 (columns with stripes; 67 cells) after each step of serial rehydration with SE bars. The **ΔΣ** was preserved during serial rehydration in this models. Representative PWS images of the same cells [M248 (B) and A2780 (C)] after each step of serial rehydration. All scale bars are 8 μm. **** $p<0.001$.
(TIF)

S3 Fig. The effects of direct air drying on ΔΣ in HeLa model under varied humidity. Representative images of HeLa model air dried in (A) 25% (±5%), (B) 50% (±5%) and (C) 75% (±5%) humidity. (D) Quantification of mean nuclear Σ (25% humidity: HeLa-control = 67 cells, HeLa-daunorubicin = 72 cells; 50% humidity: HeLa-control = 131 cells, HeLa-daunorubicin = 141 cells; 75% humidity: HeLa-control = 135 cells, HeLa-daunorubicin = 126 cells) with SE bars. All scale bars are 11 μm. **** $p<0.001$, * $p = 0.01$.
(TIF)

S1 File. Supplementary information. Supplementary information file with additional details and explanation of the PWS system, acquisition and analysis procedures, and the meaning of Σ.
(DOCX)

S2 File. A2780 STR profile. Short Tandem Repeat (STR) analysis of the A2780 derived cell line used in these studies.
(PDF)

S3 File. M248 STR profile. Short Tandem Repeat (STR) analysis of the A2780.m248 derived cell line used in these studies.
(PDF)

S4 File. Data file. Prism data file containing all the individual cell data used to produce the statistics and figures included in the manuscript.
(PZFX)

Acknowledgments

We thank Di Zhang for support and critical discussions.

Author Contributions

Conceptualization: Xiang Zhou, Scott Gladstein, Luay M. Almassalha, Yue Li, Lusik Cherkezyan, Hariharan Subramanian, Vadim Backman.

Formal analysis: Xiang Zhou.

Funding acquisition: Igal Szleifer, Vadim Backman.

Investigation: Xiang Zhou, Luay M. Almassalha, Yue Li, Adam Eshein, Parvathi Viswanathan.

Methodology: Xiang Zhou, Scott Gladstein, Hariharan Subramanian.

Project administration: Scott Gladstein, Luay M. Almassalha, Hariharan Subramanian, Vadim Backman.

Resources: Xiang Zhou.

Supervision: Scott Gladstein, Luay M. Almassalha, Lusik Cherkezyan, Hariharan Subramanian, Igal Szleifer, Vadim Backman.

Validation: Xiang Zhou, Scott Gladstein.

Visualization: Xiang Zhou, Scott Gladstein.

Writing – original draft: Xiang Zhou, Scott Gladstein.

Writing – review & editing: Xiang Zhou, Scott Gladstein, Luay M. Almassalha, Adam Eshein, Lusik Cherkezyan, Igal Szleifer, Vadim Backman.

References

1. Etzioni R, Urban N, Ramsey S, McIntosh M, Schwartz S, Reid B, et al. The case for early detection. Nat Rev Cancer. 2003; 3(4):243–52. https://doi.org/10.1038/nrc1041 PMID: 12671663
2. Ludwig JA, Weinstein JN. Biomarkers in Cancer Staging, Prognosis and Treatment Selection. Nat Rev Cancer. 2005; 5(11):845–56. https://doi.org/10.1038/nrc1739 PMID: 16239904
3. Creech MK, Wang J, Nan X, Gibbs SL. Superresolution Imaging of Clinical Formalin Fixed Paraffin Embedded Breast Cancer with Single Molecule Localization Microscopy. Sci Rep. 2017; 7:40766. https://doi.org/10.1038/srep40766 https://www.nature.com/articles/srep40766#supplementary-information. PMID: 28098202
4. Eldridge WJ, Steelman ZA, Loomis B, Wax A. Optical Phase Measurements of Disorder Strength Link Microstructure to Cell Stiffness. Biophys J. 2017; 112(4):692–702. Epub 2017/03/04. https://doi.org/10.1016/j.bpj.2016.12.016 PMID: 28256229; PubMed Central PMCID: PMC5340128.
5. Takabayashi M, Majeed H, Kajdacsy-Balla A, Popescu G. Tissue spatial correlation as cancer marker: SPIE; 2019. 6 p.
6. Subramanian H, Pradhan P, Liu Y, Capoglu IR, Li X, Rogers JD, et al. Optical methodology for detecting histologically unapparent nanoscale consequences of genetic alterations in biological cells.

Proceedings of the National Academy of Sciences. 2008; 105(51):20118–23. https://doi.org/10.1073/pnas.0804723105 PubMed Central PMCID: PMC2629261. PMID: 19073935

7. Roy HK, Turzhitsky V, Kim Y, Goldberg MJ, Watson P, Rogers JD, et al. Association between rectal optical signatures and colonic neoplasia: potential applications for screening. Cancer Res. 2009; 69 (10):4476–83. Epub 2009/05/05. https://doi.org/10.1158/0008-5472.CAN-08-4780 PMID: 19417131.
8. Radosevich AJ, Mutyal NN, Yi J, Stypula-Cyrus Y, Rogers JD, Goldberg MJ, et al. Ultrastructural alterations in field carcinogenesis measured by enhanced backscattering spectroscopy. J Biomed Opt. 2013; 18(9):097002–. Epub 2013/09/05. https://doi.org/10.1117/1.JBO.18.9.097002 PMID: 24008865.
9. Cherkezyan L, Stypula-Cyrus Y, Subramanian H, White C, Dela Cruz M, Wali RK, et al. Nanoscale changes in chromatin organization represent the initial steps of tumorigenesis: a transmission electron microscopy study. BMC cancer. 2014; 14:189. Epub 2014/03/19. https://doi.org/10.1186/1471-2407-14-189 PMID: 24629088; PubMed Central PMCID: PMC3995586.
10. Wax A, Yang C, Backman V, Badizadegan K, Boone CW, Dasari RR, et al. Cellular Organization and Substructure Measured Using Angle-Resolved Low-Coherence Interferometry. Biophys J. 2002; 82 (4):2256–64. https://doi.org/10.1016/S0006-3495(02)75571-9 PMID: 11916880
11. Li Y, Almassalha LM, Chandler JE, Zhou X, Stypula-Cyrus YE, Hujsak KA, et al. The effects of chemical fixation on the cellular nanostructure. Exp Cell Res. 2017. http://dx.doi.org/10.1016/j.yexcr.2017.06.022.
12. Yang F, Teves SS, Kemp CJ, Henikoff S. Doxorubicin, DNA torsion, and chromatin dynamics. Biochimica et biophysica acta. 2014; 1845(1):84–9. https://doi.org/10.1016/j.bbcan.2013.12.002 PMC3927826. PMID: 24361676
13. Guo N, Puhlev I, Brown DR, Mansbridge J, Levine F. Trehalose expression confers desiccation tolerance on human cells. Nat Biotechnol. 2000; 18(2):168–71. https://doi.org/10.1038/72616 PMID: 10657122
14. Eroglu A, Russo MJ, Bieganski R, Fowler A, Cheley S, Bayley H, et al. Intracellular trehalose improves the survival of cryopreserved mammalian cells. Nat Biotechnol. 2000; 18(2):163–7. https://doi.org/10.1038/72608 PMID: 10657121
15. Zhao H, Brown Patrick H, Schuck P. On the Distribution of Protein Refractive Index Increments. Biophys J. 2011; 100(9):2309–17. https://doi.org/10.1016/j.bpj.2011.03.004 PMID: 21539801
16. Almassalha LM, Bauer GM, Chandler JE, Gladstein S, Cherkezyan L, Stypula-Cyrus Y, et al. Label-free imaging of the native, living cellular nanoarchitecture using partial-wave spectroscopic microscopy. Proc Natl Acad Sci U S A. 2016; 113(42):E6372–E81. https://doi.org/10.1073/pnas.1608198113 PMC5081614. PMID: 27702891
17. Cherkezyan L, Zhang D, Subramanian H, Capoglu I, Taflove A, Backman V. Review of interferometric spectroscopy of scattered light for the quantification of subdiffractional structure of biomaterials. BIOMEDO. 2017; 22(3):030901–. https://doi.org/10.1117/1.JBO.22.3.030901 PMID: 28290596
18. Cherkezyan L, Capoglu I, Subramanian H, Rogers JD, Damania D, Taflove A, et al. Interferometric spectroscopy of scattered light can quantify the statistics of subdiffractional refractive-index fluctuations. Phys Rev Lett. 2013; 111. https://doi.org/10.1103/PhysRevLett.111.033903 PMID: 23909326
19. Cherkezyan L, Subramanian H, Backman V. What structural length scales can be detected by the spectral variance of a microscope image? Opt Lett. 2014; 39(15):4290–3. https://doi.org/10.1364/OL.39.004290 PubMed Central PMCID: PMC4317340. PMID: 25078159
20. Almassalha LM, Tiwari A, Ruhoff PT, Stypula-Cyrus Y, Cherkezyan L, Matsuda H, et al. The Global Relationship between Chromatin Physical Topology, Fractal Structure, and Gene Expression. Sci Rep. 2017; 7:41061. https://doi.org/10.1038/srep41061 PMC5259786. PMID: 28117353
21. Hobro AJ, Smith NI. An evaluation of fixation methods: Spatial and compositional cellular changes observed by Raman imaging. Vib Spectrosc. 2017; 91:31–45. http://dx.doi.org/10.1016/j.vibspec.2016.10.012.
22. Purea A, Webb AG. Reversible and irreversible effects of chemical fixation on the NMR properties of single cells. Magn Reson Med. 2006; 56(4):927–31. https://doi.org/10.1002/mrm.21018 PMID: 16941621
23. Chen F, Kan H, Castranova V. Chapter 10—Methylation of Lysine 9 of Histone H3: Role of Heterochromatin Modulation and Tumorigenesis† A2—Tollefsbol, Trygve. Handbook of Epigenetics. San Diego: Academic Press; 2011. p. 149–57.